Materials Research Proceedings 41 (2024) 390-397 https://doi.org/10.21741/9781644903131-44

Experimental and computational analysis of 3D printed 2D lattices

MUSSINI Andrea[1], CARTER Luke[2], VILLAPUN Victor[2], CAO Emily[2], COX Sophie[2] and GINESTRA Paola[1,a *]

[1]Department of Mechanical and Industrial Engineering, University of Brescia, Via Branze, 38 25123 Brescia, Italy

[2] School of Chemical Engineering, College of Engineering and Physical Sciences, University of Birmingham, Edgbaston, B15 2TT, United Kingdom

[a]paola.ginestra@unibs.it

Keywords: Lattice Structures, Metamaterials, Mechanical Simulations

Abstract. Additive Manufacturing can offer different solutions in terms of bespoke implants and deformable structures tailorable by the geometry design. The prototyping phase consists in a preliminary evaluation of the mechanical performances to find a relation with the geometrical parameters. For these reasons, numerical tools that can relate directly the geometrical features, especially for lattice or cellular structures, to the mechanical properties, are often studied to speed up the design and production process. In this study, the predictability of the deformation of a structure composed by honeycomb unit cells was studied performing compression simulations. Successively, the structure was 3D printed using fused filament fabrication and tested using a positioning stage, the relative displacements of 36 specific points of the structure were extracted using contactless measurement techniques and compared with the simulations. The results demonstrated a good predictability of the model in relation to the deformation of the structure with a stable relationship between the geometry selected and the final mechanical properties.

Introduction

Additive Manufacturing (AM) is a process used to produce highly complex parts that would otherwise require expensive processing. Because of the ability to produce complex geometric parts starting from medical imaging data and the possibility to use biocompatible materials, AM is rapidly becoming one of the most studied techniques for orthopaedic applications [1] especially cranial plates [2]. The main advantage of AM is the possibility to tune the structure depending on the patient specific needs, geometry and pathology [3].

Metamaterials are being extensively studied due to their capacity to defy the limitations of traditional materials, offering tailored and exceptional mechanical properties. These engineered materials are designed at a smaller scale, granting the ability to exhibit characteristics not commonly found in natural substances. By manipulating their structures and compositions, metamaterials can display properties like negative Poisson's ratios, negative mass density, or properties that can be finely tuned. Their response to stress and strain is unconventional, providing opportunities for applications in vibration damping, impact resistance, and even cloaking of mechanical waves. Moreover, these materials can be incredibly lightweight yet possess remarkable mechanical strength, offering valuable solutions in weight-sensitive industries like aerospace and automotive sectors. Metamaterials can achieve extreme mechanical properties, surpassing those found in conventional materials, and their structural flexibility and adaptability allow for tailoring responses to varying conditions. These unique mechanical characteristics open doors to novel applications, from next-generation mechanical components to advanced robotics and innovative medical devices, where custom-designed mechanical behavior is crucial.

Materials Research Proceedings 41 (2024) 390-397 https://doi.org/10.21741/9781644903131-44

In the biomedical context, metamaterials have also played an important role in the development of structures with advanced functionalities [4,5], these materials are able to obtain specific mechanical (Young modulus, Poisson's ratio) and biological properties with a smart design of the small-scale architecture of the system. This smart use of the design at the unit cell level can also be used to improve implant fixation [6]. Numerical modelling of mechanical tests involves computational methods to simulate and analyse how materials respond to compression forces. It's a vital aspect of understanding material behaviour and predicting mechanical properties without solely relying on physical testing.

Finite Element Analysis (FEA) is a primary technique used in this modelling. It involves breaking down complex structures or materials into smaller, manageable elements to simulate their response to compression. This method predicts stress, strain, and deformation. Defining accurate boundary conditions is essential for simulation accuracy. This includes specifying the type of compression load applied to the material, whether it's uniaxial, confined, or any other form of loading. One key aspect is the validation and calibration of models against real experimental data [7].

This ensures that the simulations accurately represent the behaviour of the material under compression. Various software tools are employed for creating models, applying loads, defining material properties, and analysing results. These tools offer a platform for conducting detailed simulations and each tool is different in terms of computational costs and accuracy of the model. While numerical modelling offers cost and time-saving benefits, there are challenges. Accurately characterizing materials and selecting appropriate models, validating simulations against real-world data, and managing computational costs for complex models are key among these challenges.

In this paper, a 2D lattice honeycomb structure was designed in Solidworks (version 2021, ©2002-2023 Dassault Systèmes) varying general starting parameters to accommodate the chosen manufacturing process. Compression simulations were performed using Solidworks and the data regarding the displacement in the XY field of 36 specific points were extracted. The structure was then 3D printed and tested. The compression of the structure was recorded using a camera at 24 FPS the deformation of thirty six specific points in the structure was tracked. The tracked displacement of the points was compared with the results obtained in the simulations and the Poisson's ratio of the structure was calculated.

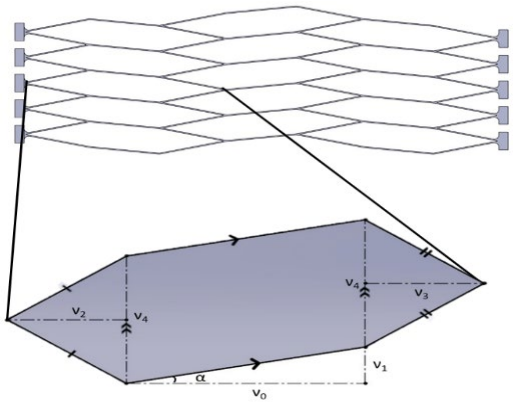

Figure 1. Tested structure and parameters definition.

The predictability of the deformation of the lattice sample in Fig 1, produced through fused filament fabrication (FFF) of polylactic Acid (PLA), has been analysed using a contactless data extraction method to obtain the relative displacement of specific points of the structure.

Materials Research Proceedings 41 (2024) 390-397 https://doi.org/10.21741/9781644903131-44

Materials and Methods

In order to be able to study the deformation of the honeycomb net structure, and assess its predictability, a compression simulation was first conducted (Fig. 2 a and b). Then, three replicas of the structure were 3D printed and physically tested, to validate the computational simulations with the acquired displacement of the trigger points (Fig. 2 c and d). Two different type of validation tests were made, one to test the behaviour of the structure under multiple consecutive compressions and assess the repeatability of the experiment, and the second to test if any differences were present between two identical nets to assess the building process reliability and repeatability.

For the experimental tests, the extremities of the structure were fully locked for two reasons: the first is that even though the calculation of the Poisson's ratio usually requires free edges, we were not able to obtain a compression system that allowed for free and frictionless movement of the edges in the Y direction (Fig. 2 c), the second reason was that these locked edges tests are more similar to the envisioned use of the device, where the structure would be ideally attached to the patient's skull. Moreover, two different angle α, defined as arctan(v1/v0), were tested to define a parametrical system.

Simulation of the compression tests. The starting parameters of the base unit cell were: v0 = v2 = v3 = 30 mm; v1 = 3.75 mm; v4 = 15 mm with a wall thickness of 0.6 mm and a height of 4 mm (Fig. 1 and Fig. 2a). These parameters were chosen as they could reliably be manufactured to enable a direct comparison between simulations and experiments. Simulations were conducted in Solidworks (version 2021, ©2002 - 2023 Dassault Systèmes) where custom material properties were inserted based on the PLA filament datasheet (Prusa) and literature [8]. The Von Mises-plasticity model was employed. The left side of the structure was then fully constrained and a displacement of -6mm was imposed on the right side in the X direction (Fig. 2b) as a boundary condition. The XY displacements of 36 points positioned at the structural nodes were extracted and subsequently compared to the experimental results.

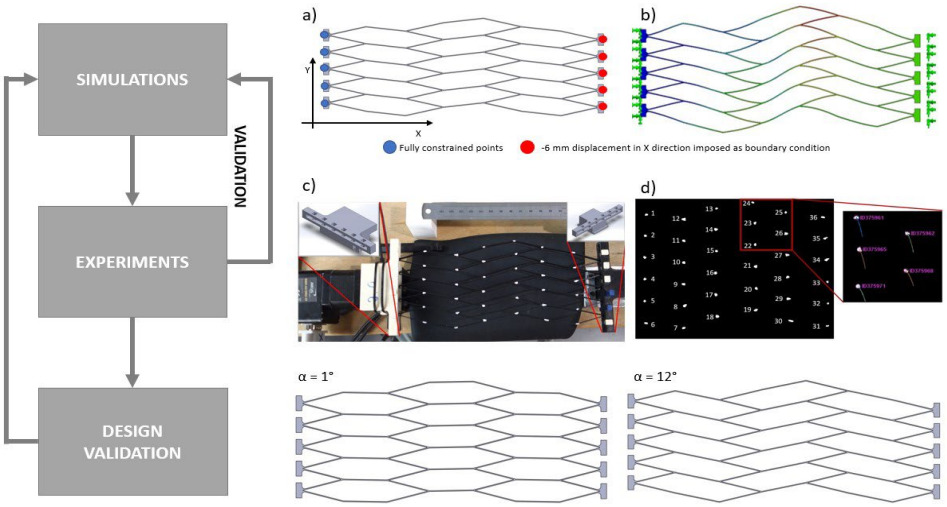

Figure 2. Flow chart of the work performed, with some deepenings on the position of constrains in the simulation, the experimental setup and data extraction and some other structures.

Manufacturing of the structure via FFF. The structures were produced using a FFF modelling system (MK3, Prusa© Prusa Research a.s.) equipped with a 0.4mm nozzle. Each structure was designed in Solidworks (version 2021), exported in .stl files and imported in the slicing software PrusaSlicer (version 2.4.2) to generate the Gcode, the filament used was the Prusament PLA Prusa

Galaxy Black filament. An infill of 100% was chosen, the nozzle temperature was 125° and the bed temperature was 60°.

Experimental compression tests. To allow the comparison with the simulations results, the 36 points at the structural nodes (average diameter 2.5 mm) were painted on the structure using white paint (Fig. 2c), and compression tests were performed using a bespoke Velmex XSlide positioning stage powered by an Arcus DMX-A2-DRV-17 engine. The locking mechanism allowed the study of the deformation of the structure by providing two planes that were at the same height in relation to the ground, on top of which the edges were located to assure the stability of the structure during the test. The locking mechanism was also 3D printed (Fig. 2c). The locking mechanism was attached to the positioning stage and the structure was firmly locked in place using pins that did not allow movement in the Y direction, while the locking mechanism itself prevented the free movement in the XZ axis. A compression of 6mm was imposed (resolution of 1 mm/10.000 steps), with an acceleration of 0,03 mm/s2 until a speed of 1 mm/s was reached. The movement of the structure, and the subsequent displacement of the points, were recorded using a HD Philips camera at 24 frames per second held above the positioning stage by a tripod. The recording started 1s before the start of the compression and was stopped 1s after the compression ended. To obtain a clear contrast between the white dots present on the structure and the background, a plastic black mat was positioned under the structure, above the moving thread.

Data extraction and analysis. Data extraction was performed starting from the recording of the compression tests using Fiji (ImageJ) [9] and the track mate plugin [10]. The recording was imported in ImageJ as an image stack with 165 frames containing the compression, at the same time the image stack was cropped to show only the structure. Subsequently, a binary thresholding was performed on the stack to show only the white reference dots (Fig. 2d). Using the Trackmate plugin, the displacement of each of the 36 dots was extracted. The Difference of Gaussians (DoG) detector was used selecting an object diameter of 3 mm and a quality threshold of 6, to allow tracking of the 36 points with no interference. To track the points, the simple linear assignment problem (LAP) tracker was selected, with a linking max distance of 3 mm and a max frame gap of 6. This allowed to track all the 36 points during the movement avoiding possible track loss from the software. The obtained data were exported in a CSV file containing the track number, the frame numbers and the X,Y coordinates of the point for each of the analysed frames. The mean displacement was then calculated for each point, firstly by averaging the relative displacement frame by frame of the three compression tests performed on a structure, and then by calculating the average of all three replicas. Then standard deviation (STD) and the standard error of estimate (σest) were also calculated. The standard error of estimate was found using the following formula:

$$\sigma est = \sqrt{\frac{\sum (Y - Y')^2}{N}} \quad (1)$$

Results

Localized deformation analysis. The location of the points that were painted on the net with white paint visible in Fig. 3. This aspect has a significant effect on the simulation results and the experimental tests replicability. Three regions were identified, where all the points exhibited similar behaviours when compared to the simulations. Points 1-6 (Fig. 3 - blue region) and 31-36 (Fig. 3 - red region) located at the structure edges, demonstrated large variations between the simulations and physical test data (up to 400%). The displacements results of Point 2 and 22 were reported in Fig. 3 as references for the behaviour of the other points of the external columns. Despite the big difference in percentage values between the simulated values and the tested results, the overall relative displacement of these points is usually less than 0.2 mm, thus the error resulting

from these regions should not affect the points in the central yellow region. For these reasons, more emphasis was placed on a comparison between the simulation results and the experimental results of points 7 – 30 that were located further from the edges of the structure, in the central region (Fig. 3 – yellow region).

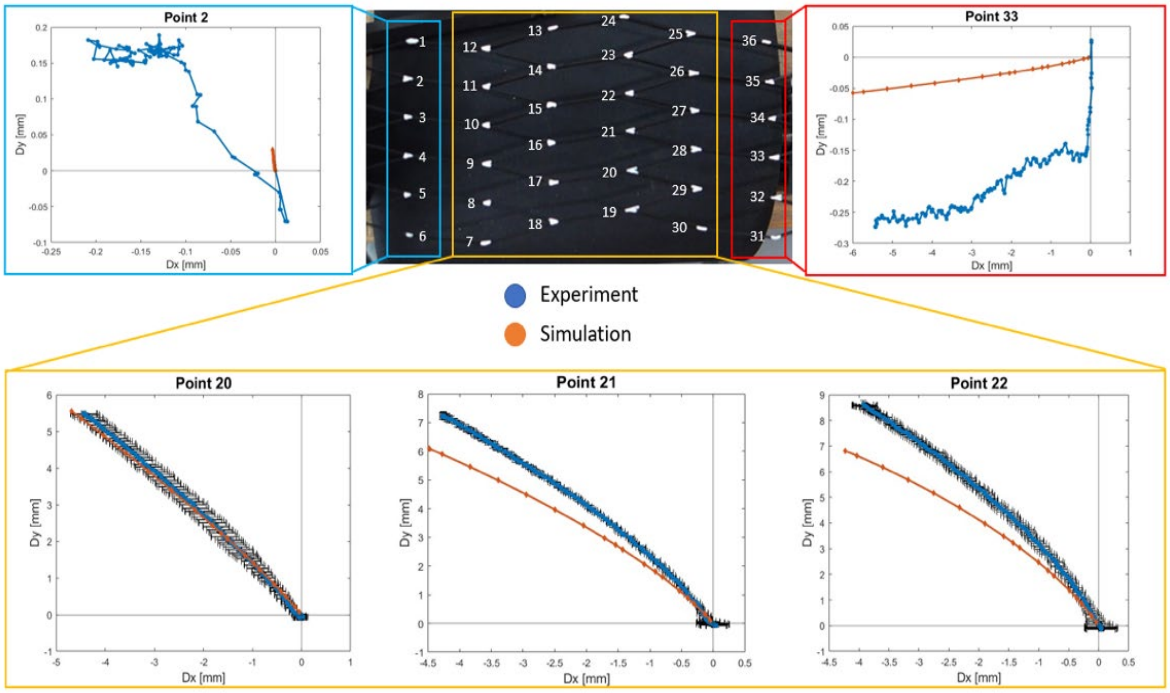

Figure 3. Points comparison between simulations and experiments, the analysis led us to discard points between 1 and 6 and between 31 and 36 because of how unpredictable they were, points from 7 to 30 showed a trend that was closer to the expected one.

Standard error of estimate. For each of the points in the central yellow region (indicated by the yellow box in Fig. 3), the average displacement and standard error of estimate (σest) were calculated (Fig. 4). Among the three repetitions of the structures with an α value of 7.125°, clear trends of points that exhibited the highest and lowest variation were noticed. Specifically, points 7, 18, 19, 23, 24 and 25 had error values between 1 and 1.8 while for the remaining points the dataset were strongly correlated with σest below 0.8. Among the three replicas, Structure 1 (Fig. 4a) is the one with the lowest σest in all points, with most points showing a value under 0.8; structure 2 (Fig. 4b) is the one with the highest σest in all points but with values of σest<1.2 for most of the points; andStructure 3 (Fig. 4b) being much closer to the average of the three structures combined (Fig. 4d). The average value of σest of the three structures combined is 0.687.

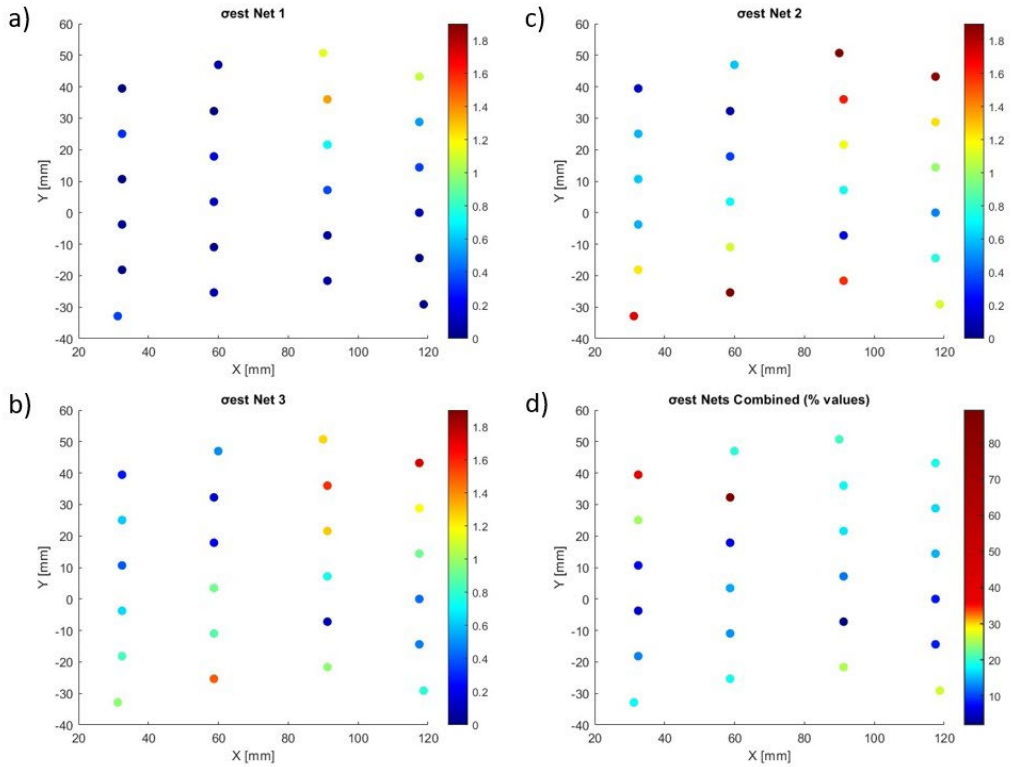

Figure 4. Standard Error of Estimate of three physical repeats of the structure (α=7.125°) (a, b, c) and the combined values of the three (d).

Fig. 5 (a and b) shows the values of the standard deviation (STD) expressed in % values of the combination of the three replicas. For the X axes, the values are below 10% (Fig. 5a) for 21 of the 24 examined points, notable outliers are present such as points 14, 19 and 30 having STD values between 30% and 60%. In Fig. 5b representing the Y axes, it can be noticed that the values of the STD fall under 10% with no notable outliers. Fig. 5c allows to understand the values in a clearer way, for example points 23, 24, 25 that appear to have a higher absolute σest values compared to the rest of the points, are more similar to the other points when the percentage values are observed. The average error in Fig. 5c is 23.86% with points 12 and 14 being outliers with error values over 100%. This error can be imputed to the small total deformation that these two points show, the value of the relative displacement in the y axis is in fact less than 1 mm in both points.

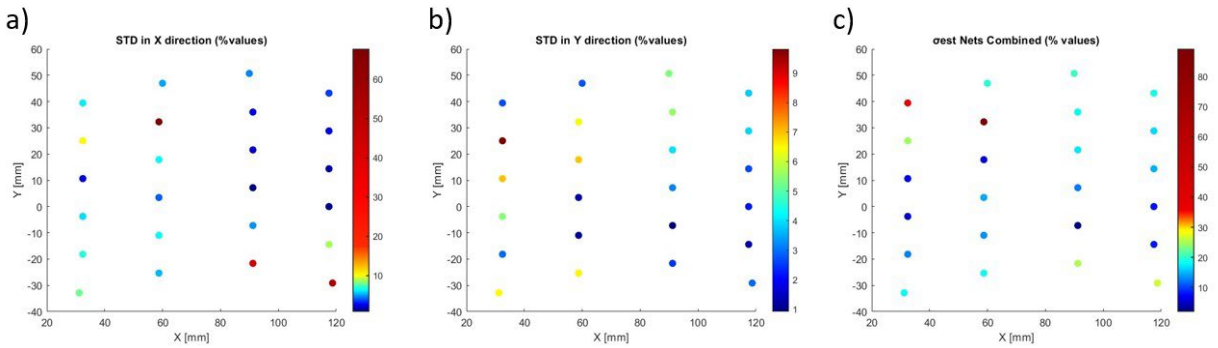

Figure 5. Standard Deviation values for the three structures combined both in the X direction (a) and in the Y direction (b); (c) shows the % values of the Standard Error of Estimation of the graph present in Fig. 4d.

Discussion and Conclusions

In Fig. 3 it is possible to notice two main areas where the experimental results do not coincide with the simulations, those two areas are points 1-6 and 31-36 that were very close to the locking mechanism. The instability of the two areas closest to the edges is an indicator that the locking mechanism introduced some instabilities at the edges, specifically during the starting phase of the compression where it is possible to notice the biggest displacement of those points. However, despite this instability, the displacement of the points remains for most of them less than 0.2mm, where for the other points the displacement is usually of several millimeters. Therefore, the error introduced by these points has no impact on the points in the central area that show high levels of displacement accuracy.

In Fig. 4 (a,b and c) it is noticeable how, despite showing the same trend on the points with the highest error, Net 1 is characterized by an overall standard error of estimate lower than Nets 2 and 3. This can be due to a better locking achieved during the testing phase of Net 1 compared to Nets 2 and 3. The three structures all show comparable values when it comes to σest, indicating that the FFF process does not lead to significant differences between different structures produced with the same equipment. Moreover, the performed simulations align closely with the experimental results obtained with the positioning stage with a prediction error in the Standard Error of Estimate below 20% for most points, and a standard deviation usually below 10%, indicating the similarity of the results to the real-life situation. The visual comparison between the videos of the deformed structure and the simulations also shows a very similar deformed configuration between the simulations and the compression tests, in accordance with the average error observed in other studies of lattice structures [11,12,13] where errors ranging from 7.4% and 28.2% are reported between the predicted and tested stress-strains curves. In general, AM structures show to be less stiff than the simulated structures, leading to higher deformations than expected. These results show not only that the production process is reliable, but also that the used extraction data process is reliable, and it could be used in future works to extract data from other deformable structures without contact: TrackMate is an already established addon to Fiji (ImageJ) that is used in various fields for single particle tracking [14] and for automatic cell tracking [15]. This study demonstrates that it is also possible to study the displacement of specific points within a structure in reliable way.

References

[1] P. Ginestra, S. Pandini, E. Ceretti, Hybrid multi-layered scaffolds produced via grain extrusion and electrospinning for 3D cell culture tests, Rapid Prototyping Journal, 26(3), 2019, 593–602.

[2] J. Banks, Adding Value in Additive Manufacturing : Researchers in the United Kingdom and Europe Look to 3D Printing for Customization, in IEEE Pulse, vol. 4, no. 6, pp. 22-26, Nov. 2013. https://doi.org/10.1109/MPUL.2013.2279617

[3] H. Dodziuk, Applications of 3D printing in healthcare. Kardiochirurgia i Torakochirurgia Polska/Polish Journal of Thoracic and Cardiovascular Surgery, 2016;13(3):283-293. https://doi.org/10.5114/kitp.2016.62625

[4] A.A. Zadpoor, Mechanical meta-materials, Mater. Horizons, 3 (5) (2016), pp. 371-381

[5] C.P. de Jonge, H.M.A. Kolken, A.A. Zadpoor, Non-Auxetic Mechanical Metamaterials, Materials. 2019; 12(4):635. https://doi.org/10.3390/ma12040635

[6] H.M.A. Kolken, C.P. de Jonge, T. van der Sloten, A. Fontecha Garcia, B. Pouran, K. Willemsen, H. Weinans, A.A. Zadpoor, Additively manufactured space-filling meta-implants, Acta Biomaterialia, Volume 125, 2021, Pages 345-357, ISSN 1742-7061, https://doi.org/10.1016/j.actbio.2021.02.020

[7] D. Gastaldi, G. Parisi, R. Lucchini, S. Bignozzi, P.S. Ginestra, G. Filardo, R. Contro, E.Kon, P.Vena, A Predictive Model for the Elastic Properties of a Collagen-Hydroxyapatite Porous Scaffold for Multi-Layer Osteochondral Substitutes, International Journal of Applied Mechanics; Vol. 7, No. 4 (2015) 1550063.

[8] S. Farah, D.G. Anderson, R. Langer, Physical and mechanical properties of PLA, and their functions in widespread applications — A comprehensive review, Advanced Drug Delivery Reviews, Volume 107, 2016, Pages 367-392, ISSN 0169-409X.

[9] J. Schindelin, I. Arganda-Carreras, Frise, E., et. al. Fiji: an open-source platform for biological-image analysis. Nature Methods, 9(7), (2012), 676–682. https://doi.org/10.1038/nmeth.2019

[10] Ershov, D., Phan, M.-S., Pylvänäinen, J. W., Rigaud, S. U., Le Blanc, L., Charles-Orszag, A., … Tinevez, J.-Y. (2022). TrackMate 7: integrating state-of-the-art segmentation algorithms into tracking pipelines. Nature Methods, 19(7), 829–832. https://doi.org/10.1038/s41592-022-01507-1

[11] A.M. Abou-Ali, O. Al-Ketan, Dong-Wook Lee, Reza Rowshan, Rashid K. Abu Al-Rub, Mechanical behavior of polymeric selective laser sintered ligament and sheet based lattices of triply periodic minimal surface architectures, Materials & Design, Volume 196, 2020, 109100, ISSN 0264-1275.

[12] Shuai Ma, Qian Tang, Xiaoxiao Han, Qixiang Feng, Jun Song, Rossitza Setchi, Ying Liu, Yang Liu, Athanasios Goulas, Daniel S. Engstrøm, Yau Yau Tse, Ni Zhen, Manufacturability, Mechanical Properties, Mass-Transport Properties and Biocompatibility of Triply Periodic Minimal Surface (TPMS) Porous Scaffolds Fabricated by Selective Laser Melting, Materials & Design, Volume 195,2020, 109034, ISSN 0264-1275.

[13] Mohammadreza Moeini, Mickael Begon, Martin Lévesque, Numerical homogenization of a linearly elastic honeycomb lattice structure and comparison with analytical and experimental results, Mechanics of Materials, Volume 167, 2022, 104210, ISSN 0167-6636.

[14] Jean-Yves Tinevez, Nick Perry, Johannes Schindelin, Genevieve M. Hoopes, Gregory D. Reynolds, Emmanuel Laplantine, Sebastian Y. Bednarek, Spencer L. Shorte, Kevin W. Eliceiri, TrackMate: An open and extensible platform for single-particle tracking,Methods, Volume 115, 2017, Pages 80-90, ISSN 1046-2023, https://doi.org/10.1016/j.ymeth.2016.09.016

[15] Fazeli, E., Roy, N. H., Follain, G., Laine, R. F., von Chamier, L., Hänninen, P. E., Eriksson, J. E., Tinevez, J. Y., & Jacquemet, G. (2020). Automated cell tracking using StarDist and TrackMate. F1000Research, 9, 1279. https://doi.org/10.12688/f1000research.27019.1